analytical chemistry

pubs.acs.org/ac Article

Organic Field-Effect Transistor-Based Biosensors with Enhanced Sensitivity and Reliability under Illumination for Carcinoembryonic Antigen Bioassay

Xue Wang, Chenfang Sun, Congcong Zhang, Shanshan Cheng,* and Wenping Hu

Cite This: *Anal. Chem.* 2021, 93, 15167−15174 Read Online

ACCESS | Metrics & More | Article Recommendations | Supporting Information

ABSTRACT: Achieving biosensors of high sensitivity and reliability is extremely significant for early diagnosis and treatment of tumor diseases. Herein, a novel organic field-effect transistor (OFET)-based biosensor was developed and applied for carcinoembryonic antigen (CEA) bioassay. This OFET-based biosensor can respond sensitively to the antigen−antibody immune-recognition reaction under illumination and darkness, respectively, thereby generating electrical signal changes of source-drain current (I_{DS}) and threshold voltage (V_{th}). The OFET-based biosensor exhibits detection limits for CEA detection of 0.5 and 0.2 pM, respectively, using I_{DS} and V_{th} as the response signals under darkness. When a specific intensity of light is applied, light will influence the charge-carrier transport process in the conductive channel, thus causing biosignals to turn into higher electrical signal changes of photocurrent and threshold voltage under illumination. Compared with the detection results in the dark, the biosensor exhibits higher sensitivity for CEA detection under illumination with detection limits of 13.5 and 16.9 fM. Also, multisignal outputs effectively improve the reliability of the biosensor for CEA detection. Consequently, with powerful detection functions, this OFET-based biosensor is expected to become a high-performance biosensing platform for the detection of various biological substances in the future.

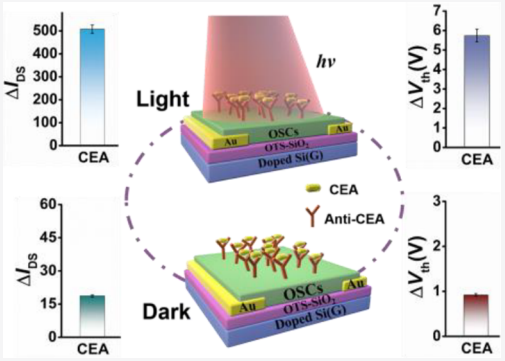

INTRODUCTION

Highly sensitive and reliable determination of biological analytes plays a significant role in the early diagnosis, real-time monitoring, and treatment of disease.[1−3] Organic field-effect transistor (OFET)-based biosensors[4−7] that emerged in recent years have attracted more and more attention from researchers. The OFET-based biosensors have many advantages such as easy large-area preparation, miniaturization, integration, small size, low cost, and fast response speed. To improve the bioassay capability of OFET-based biosensors, researchers have adopted a variety of strategies to design and construct innovative types of sensors.[8,9] For example, functional modification of the sensing interface can enhance the interaction of analyte and biosensing layer so as to exhibit higher sensitivity and reduce the detection limit.[10] Nevertheless, this method has problems such as a complex surface-modification process with great difficulty and an inevitable impact on the electrical performance of the device. Other methods include synthesizing organic semiconductor materials with specific functional groups for better identification of analytes or developing new device structures to improve sensor performance.[11,12] However, they may face problems such as difficult synthesis paths, cumbersome manufacturing processes, and operational difficulties. In addition, accurate and reliable detection of biological substances is essential for disease diagnosis. Therefore, some researchers had designed biosensors[13−16] with two different signal-transduction mechanisms to realize a multisignal readout biosensor. Moreover, the preparation process of this biosensor was simple, and powerful detection functions could be obtained. Biosensors with multisignal outputs[17−19] can mutually verify the detection results of different signals, which will enhance the accuracy and reliability of the detection results.

The organic semiconductor components applied to construct OFET-based biosensors are generally utilized to sense charged biomolecules, and the detection of biological analytes is realized by reading electrical signals changes of the OFET. Currently, there are many types of semiconductors.[20] Moreover, polymer organic semiconductors have advantages of biocompatibility, easy solution processing, and other characteristics[21−24] that make them have great application prospects as biosensing platforms. Because organic semiconductors with good photoelectric activity are sensitive to light, light can

Received: August 26, 2021
Accepted: October 21, 2021
Published: November 1, 2021

influence the charge-carrier transport process in the conductive channel.[25−28] Therefore, the OFET based on photoactive semiconductor materials constitutes a biosensor, which exhibits higher sensitivity for biological-analyte detection under light illumination.[29,30] Furthermore, the photoelectric active material can be used as an organic semiconductor layer and a biosensing layer simultaneously, which simplifies the fabrication process of the highly sensitive immunosensor.

In this study, a novel OFET-based biosensor was first constructed using diketopyrrolopyrrole-quaterthiophene (PDQT), a conjugated polymer with excellent photoelectric activity,[31,32] as the organic semiconductor material to realize the bioassay of carcinoembryonic antigen (CEA) with enhanced sensitivity and reliability (Scheme 1). The OFET-based biosensor could simultaneously obtain the signal changes of source-drain current (I_{DS}) and threshold voltage (V_{th}) caused by the specific biological immune response under illumination and in the dark. In the dark conditions, the detection limits for the CEA bioassay were 0.5 and 0.2 pM with I_{DS} and V_{th} as the response signals, respectively. Because of the regulation of the electrical signal by illumination, the biosensor has higher sensitivity for CEA detection under illumination, and the detection limits were 13.5 and 16.9 fM, respectively, with I_{DS} and V_{th} as the response signals. Multisignal outputs effectively improve the reliability of the biosensor, and the regulation of electrical signals by light illumination improves the sensitivity of the sensor for CEA bioassay, which will contribute to the sensitive and accurate determination of some trace substances. Compared with other detection methods, this OFET-based biosensor holds the advantages of small size, simple operation, and high sensitivity and reliability, and it is expected to become a high-performance sensing platform for the detection of various biological substances.

Scheme 1. Development of OFET-Based Biosensors for CEA Assay under Illumination and Darkness: (I) Fabrication of the OFET Device; (II) Construction of the Biosensing Platform; and (III) Detection of CEA

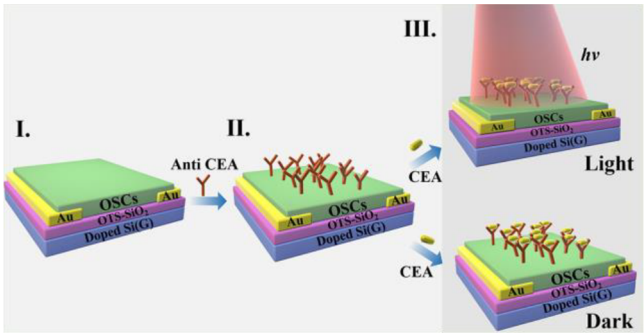

EXPERIMENTAL SECTION

Chemicals and Reagents. Monomer material DPP-38 for polymer synthesis was purchased from Shenzhen Ruixun Optoelectronic Material Technology Co., Ltd. 5,5′-Bis-(trimethylstannyl)bithiophene was purchased from Waljiming (Beijing) Technology Development Institute. Chlorobenzene was purchased from Tianjin Yuanli Chemical Co., Ltd. The chemical reagents used in the experiment were of analytical grade. Octadecyl trichlorosilane (OTS) was purchased from Beijing Bailingwei Technology Co., Ltd. Human serum albumin (HSA), α-fetoprotein (AFP), mouse monoclonal CEA antibody (anti-CEA antibody), and carcinoembryonic antigen (CEA) were all purchased from MyBioSource, Inc. (U.S.A.). The phosphate-buffered solution (PBS) used was manufactured in the laboratory. Ultrapure water of 18.20 MΩ·cm was utilized at room temperature.

Experimental Instruments. For evaluating the electrical characteristics of the prepared organic devices, a 4200-SCS semiconductor parameter analyzer was utilized. An MLED4-3 LED power-supply device was used to provide an 808 nm light source. The Fourier transform infrared (FT-IR) spectra before and after the immobilization of CEA antibody were obtained by a Vertex70 FT-IR spectrometer. The X-ray photoelectron spectroscopy (XPS) was executed for the evaluation of antibody immobilization by a K-Alpha X-ray spectrometer. AFM images were measured by a Dimension Icon-PT atomic force microscope (AFM, Bruker) in tapping mode. An NMR spectrometer (600 MHz, Bruker) was used to carry out the ^{1}H NMR spectrum.

Synthesis of PDQT Organic Semiconductor. The polymer PDQT was successfully synthesized by the core method in the literature[32] with a yield of 92.42%. The Supporting Information includes the detailed experimental process. The result of ^{1}H NMR spectra (Figure S1) was in accord with the previously reported result.[33] Using trichlorobenzene as the eluent, gel permeation chromatography (GPC) analysis results at 150 °C indicated that the prepared PDQT polymer was endowed with a number-average molecular weight (M_n) of 22.79 kDa and a polydispersity index (PDI) of 2.11 (Figure S2). The fabricated polymer had good thermal stability, and it was thermally decomposed at ∼400 °C (Figure S3).

Fabrication of the OFET-Based Biosensor. The OFET-based biosensor was developed on an n^+-doped silicon wafer (capacitance of ∼10.50 nF cm^{-2}) with a thermally grown SiO_2 layer (∼300 nm) using the photoelectric active material polymer PDQT as the organic semiconductor layer. First, the SiO_2/Si substrate was cleaned with piranha solution to remove the residual organic substances and to hydroxylate the surface. After oxygen-plasma treatment was performed on the silicon wafer for 10 min, the OTS monolayer was modified on the SiO_2 surface under OTS solution to increase the hydrophobicity of the SiO_2 surface. Under the cover of the copper mask, 30 nm of gold was vacuum-deposited as the gold source (S) and drain (D) electrode. Then, 5 mg mL^{-1} PDQT chlorobenzene solution was spin-coated on the OTS-treated silicon wafer to form a semiconductor layer. Afterward, the prepared device was annealed at 150 °C for 10 min to upgrade the molecular structure of the semiconductor thin film to obtain a better charge-transport performance. The channel length and width of this prepared device were 28 and 202 μm, respectively.

The fabrication process of the OFET-based biosensor is demonstrated in Scheme 1. The OFET-based device was fabricated by a simple solution method (I), and then the PDQT organic semiconductor layer was immersed in 50 μg mL^{-1} CEA antibody solution for incubation of 1 h to complete the CEA antibody immobilization process (II). Then, the surface was washed with 0.01 × PBS three times to remove unabsorbed excess CEA antibody. Finally, specific immune reactions occurred with CEA solutions of different concentrations to obtain biosensing signals (III). The control trial of other substances was the same as step III to confirm that the

https://doi.org/10.1021/acs.analchem.1c03683
Anal. Chem. 2021, 93, 15167−15174

specific CEA antibody immobilized biosensor had a good selectivity to CEA. In particular, the pH value and ionic strength of the PBS solution (approximately pH 7.4 and 10 mM, respectively) employed for the preparation of CEA solutions are similar to the environmental conditions of real samples of human serum, indicating its potential for medical detection.[34]

RESULTS AND DISCUSSION

Electrical Performance of the Organic Device under Dark Conditions. The good electrical properties of the OFET are the basis of constructing OFET-based biosensors. In Figure 1, the electrical performance of the device was characterized without light exposure using the Keithley 4200 SCS semiconductor analysis and test system. A bias gate voltage (V_G) swept from 20 to −20 V to obtain a typical transfer characteristic curve of an organic semiconductor device under a constant source-drain voltage (V_{DS} = −20 V) (Figure 1a). It was estimated from the formula $I_{DS} = W\mu C_i(V_G - V_{th})^2/2L$ that the hole mobility of the organic device was 0.291 $cm^2\ V^{-1}\ s^{-1}$ in the saturation region and its I_{on}/I_{off} ratio was 5.30×10^7. Among them, I_{DS} represents the saturation source-drain current, and C_i represents the capacitance of the SiO_2 dielectric. From the approximate linear curve fitting of the $(I_{DS})^{1/2}$ versus V_G in saturation state, it is extrapolated to the intersection with the *x*-axis, that is, the V_{th} value of the device is obtained when I_{DS} = 0. With the gate voltage change steps of −5 V, the source-drain voltage swept from 0 to −20 V to obtain the typical output characteristic curve of I_{DS} versus the source-drain voltage (Figure 1b), which indicated that the carrier was in a good charge transfer process in the conductive channel. This was also verified by the characterization of the hysteresis curve of the device (Figure S4). The mobility and V_{th} of the saturation region changed slightly in the forward and reverse scanning of V_G, which was a similar results to that of general organic semiconductors.[35,36] To further characterize the operational performance of the device, the electrical performances of 50 devices were evaluated (Figure 1c and d). Their average mobility was 0.235 $cm^2\ V^{-1}\ s^{-1}$, and the corresponding average I_{on}/I_{off} ratio was 4.61×10^7. Furthermore, as a biorecognition layer, the stability of organic semiconductors in air and aqueous solution is very significant. Owing to the structural characteristics of the diketopyrrolopyrrole (DPP)-based polymer PDQT, the long alkyl chain on the polymer surface is hydrophobic. In the previous research studies of our group,[24,37] it was demonstrated that DPP-based polymers used in OFET-based biosensors had stable electrical properties in air and water phase.

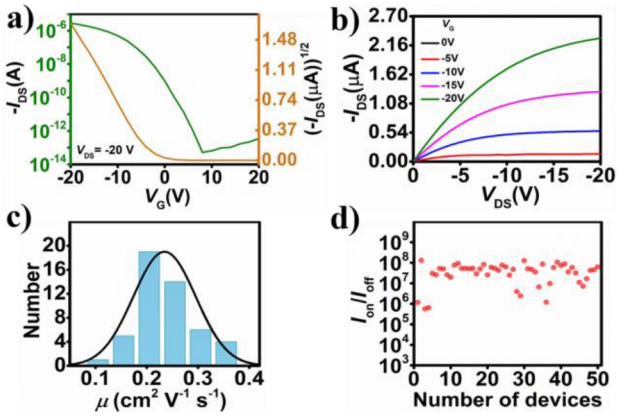

Figure 1. Electrical performance of the organic device without light irradiation. (a) Typical transfer characteristic curve of the organic device. (b) Typical output characteristic curve with a range of V_G from 0 to −20 V. (c) Mobility inthe saturation region distribution diagram of 50 devices. The average mobility was 0.235 $cm^2\ V^{-1}\ s^{-1}$. (d) Corresponding I_{on}/I_{off} ratio distribution graph of 50 devices. The average I_{on}/I_{off} ratio was 4.61×10^7.

Photoelectric Performance Measurement and Analysis of the Organic Device. The nature of the photoelectrically active material is the foundation of the photoelectric performance of the organic device. Figure 2e shows that the PDQT polymer film exhibited strong absorption in the 700−900 nm range and near-infrared light had little damage to biological substances, which was suitable for biological-substance detection. A light source of 808 nm wavelength was selected as the excitation light of the organic device, and the transfer characteristic curve of the device was measured under different light intensities (Figure 2a). The photocurrent of the device gradually increased with the increases of light intensity. The photocurrent was defined as the I_{DS} of the device obtained from the transfer characteristic curve under light-illumination conditions. Photosensitivity (P) and photoresponsivity (R)[38] are the main physical quantities used to evaluate the photoelectric performance of the organic device

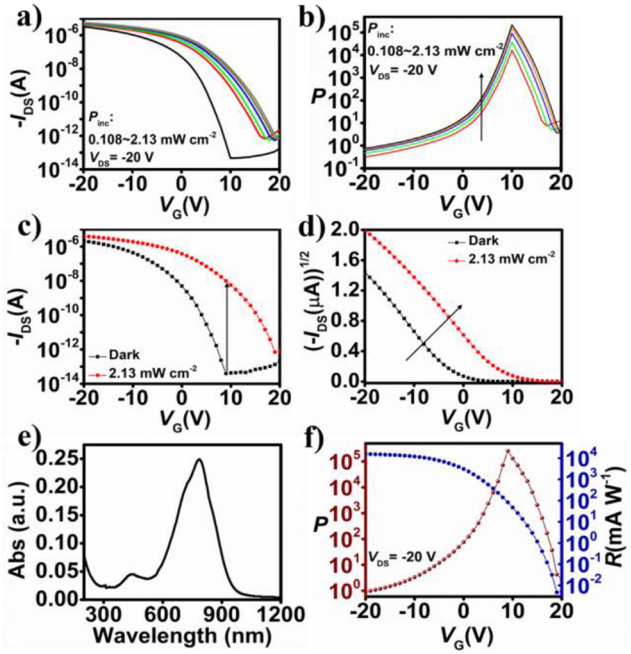

Figure 2. Characterization of optoelectronic properties of the organic device. (a) Transfer characteristic curves under different light intensities (0.108−2.13 mW cm^{-2}) of the 808 nm LED light source. (b) P versus V_G curves under different light intensities (0.108−2.13 mW cm^{-2}) of the 808 nm LED light source. (c) Transfer characteristic curves (V_{DS} = −20 V) under dark or illumination of the 808 nm LED light source with 2.13 mW cm^{-2} intensity. (d) Curves of $(-I_{DS})^{1/2}$ versus V_G (V_{DS} = −20 V) under dark or illumination of the 808 nm LED light source with 2.13 mW cm^{-2} intensity. (e) UV−vis−NIR absorption spectrum of the PDQT film. (f) Curves of P and R versus V_G (V_{DS} = −20 V) under the illumination of the 808 nm LED light source with 2.13 mW cm^{-2} intensity.

https://doi.org/10.1021/acs.analchem.1c03683
Anal. Chem. 2021, 93, 15167−15174

(see the Supporting Information). The photosensitivity (P) of the device was extracted from the formula $P = (I_{Light} - I_{Dark})/I_{Dark}$ (where I_{Light} represents the I_{DS} of the organic device under a specific illumination and I_{Dark} represents the I_{DS} of the organic device under dark conditions). With the increases of light intensity (Figure 2b), the P of the device gradually increased, showing the modulation effect of illumination on the current. As can be seen in parts c and d of Figure 2, the changes of I_{DS} and V_{th} (red line) under light conditions relative to I_{DS} and V_{th} (black line) under dark conditions indicated the potential of using I_{DS} and V_{th} as electrical-output signals for biological-substance detection under illumination. Figure 2f also describes that, under an illumination intensity of 2.13 mW cm^{-2} and a V_G of 10 V, the photosensitivity of the device was the largest, that is, the photocurrent effect was maximized. Under this condition, the photosensitivity P of the device can reach 10^5, and the maximum photoresponsivity was ~16 A W^{-1}, which had excellent performance among other organic devices (Table S1).

Therefore, the I_{DS} curve versus time was measured under the illumination intensity of 2.13 mW cm^{-2} when the source-drain voltage was −20 V and V_G was 10 V (Figure S5). I_{DS} showed almost no change over time, indicating the stability of OFET-based biosensors under illumination using I_{DS} as the electrical-output signal within sufficient biological-detection time. Also, the transfer characteristic curve of the same device was tested 20 times under illumination, from which the changes of its photosensitivity and threshold voltage (ΔP and ΔV_{th}) were obtained ($\Delta V_{th} = V_L - V_D$, where L stands for light conditions and D stands for dark conditions). The changes were small among the 20 measurements (Figure S6). These results showed the stability of the device using I_{DS} and V_{th} as electrical-output signals for biological-substance detection under light-illumination conditions.

Mechanism Explanation of OFET under Illumination and Darkness Measurements. OFET-based biosensors have been utilized to detect a variety of biological substances. Usually those charged biomolecules influenced the electrical signals by affecting the electronic properties between the interfaces to achieve label-free detection.[39−41] When the pH of the solution exceeded the isoelectric point of the protein, the protein was negatively charged. The isoelectric point (pI) of CEA is 3.40, which is lower than the pH value of the solution (~7.40). Therefore, when an antigen−antibody immune reaction occurred to form an immune complex, more negatively charged proteins were attached to the biosensing layer, promoting the generation of more carriers in the conductive channel due to electrostatic interaction. In the dark conditions of the OFET technique, the binding of negatively charged CEA with receptors on the semiconductor surface will cause the I_{DS} of the organic device to increase and the V_{th} to move in the positive direction. Because part of the carriers were captured by the traps in the channel,[42] some of the electrical-signal changes triggered by biological recognition were weakened (Figure 3a).

Under the illumination conditions of the OFET technique, the mechanism can be explained by two aspects: surface charge effect and the increase of carrier concentration.[30] When the p-type organic semiconductor material with photoelectric activity was used as the organic semiconductor layer of OFET, after a certain intensity of light was applied to the OFET, the excitons in the conductive channel dissociated to produce photogenerated carriers (holes/electrons) (Figure 3b). Driven by the

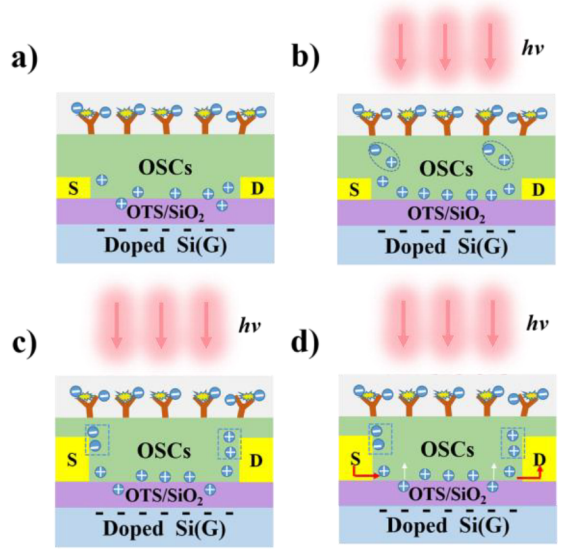

Figure 3. Mechanism explanation of the OFET-based biosensor under illumination and darkness. (a) Working principle of OFET-based biosensor for the detection of CEA in the dark. (b) Generation of photogenerated carriers of the OFET-based biosensor under light illumination. (c) Movement of photogenerated carriers in the electric field. (d) Working principle of the OFET-based biosensor for the detection of CEA under illumination (light source = 2.13 mW cm^{-2}, 808 nm).

internal electric field,[43] holes and electrons accumulated at the drain electrode and the source electrode, respectively, reducing the hole-injection barrier at the interface between the electrode and the conductive channel,[44,45] thereby indicating higher channel conductivity (Figure 3c). It was conducive to the carrier-transmission process induced by biological recognition and improved the sensitivity of biosensing. On the other hand, illumination caused the trapped holes in the channel to escape from the trap and rejoin the carrier-transport process to increase the carrier concentration caused by biological combination, increasing the I_{DS} and shifting V_{th} toward the positive direction, thereby improving the detection sensitivity (Figure 3d). Therefore, within the same gate-voltage range, the photocurrent of OFET increased and the V_{th} of OFET shifted toward the positive direction.[46,47]

Immobilization of CEA Antibody to Form a Biosensing Platform. Through the immobilization of the CEA antibody on the surface of the biosensing layer, a specific recognition interface for biosensing was constructed with the CEA antibody as a biological probe. FT-IR evaluated the immobilization process of the CEA antibody.[30] After the biosensing layer was immersed in a 50 μg/mL CEA antibody solution for 1 h incubation to form a specific recognition interface, the device was dried under nitrogen for FT-IR measurements. In Figure 4a, the N−H stretching vibration peak of $-NH_2$ appeared in the wavenumber range of 3000−3600 cm^{-1} after the immobilization of the CEA antibody. Within the wavenumber range of 1000−1500 cm^{-1}, there were the characteristic peaks of C−O and C−N bonds. Compared with the spectrum before antibody immobilization, this demonstrated the successful immobilization process of the antibody. XPS spectra (parts b and c of Figure 4) measured the O (1s) and N (1s) elements, respectively, before and after the antibody immobilization. After the immobilization of the antibody, the peak intensities of the O (1s) and N (1s)

https://doi.org/10.1021/acs.analchem.1c03683
Anal. Chem. 2021, 93, 15167−15174

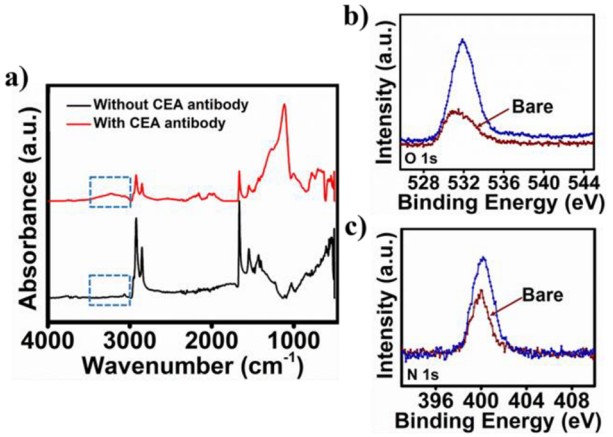

Figure 4. Characterization of CEA antibody immobilization. (a) FT-IR spectra characterization of the PDQT organic semiconductor layer before (black line) and after (red line) CEA antibody immobilization. (b) XPS spectra characterization of the O 1s peak on the surface of the PDQT biosensing layer before (red line, bare) and after (blue line) CEA antibody immobilization. (c) XPS spectra characterization of the N 1s peaks on the surface of the PDQT biosensing layer before (red line, bare) and after (blue line) CEA antibody immobilization.

elements increased significantly, which indicated that protein rich in O and N (CEA antibody), respectively, adsorbed on the surface of the biosensing layer, contributing to this phenomenon. In addition, the morphological characteristics of the PDQT polymer thin film before and after the modification of the CEA antibody were observed through an atomic force microscope (AFM).[48,49] AFM height images (Figure 5a and b) showed that, with the addition of the CEA antibody, the surface height increased from 22.51 to 30.41 nm, increasing ~8 nm, which was close to the size of the CEA antibody.[50] Meanwhile, the root-mean-square roughness of the

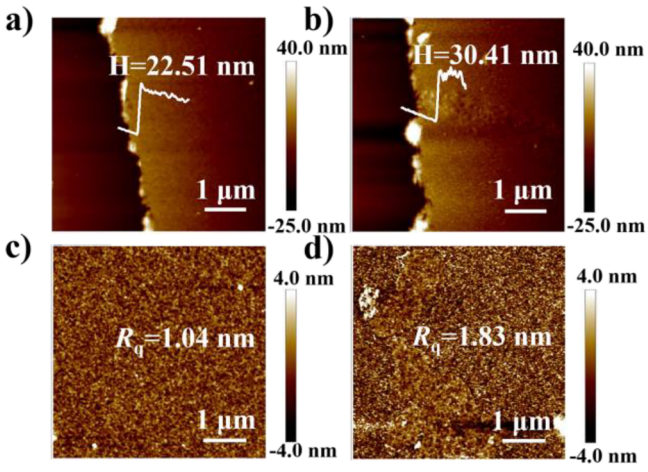

Figure 5. Observation through AFM images of the surface-morphology changes of the PDQT organic semiconductor layer before and after the immobilization of the CEA antibody. (a) Before the immobilization of the CEA antibody, the height image appeared at a surface height of 22.51 nm. (b) After the immobilization of the CEA antibody, the height image illustrated a surface height of 30.41 nm. (c) Characterization of the surface roughness (R_q = 1.04 nm) before the immobilization of the CEA antibody. (d) Characterization of the surface roughness (R_q = 1.83 nm) after the immobilization of the CEA antibody.

organic semiconductor layer (Figure 5c and d) was significantly increased from 1.04 to 1.83 nm. Therefore, the OFET-based biosensor successfully constructed a specific recognition platform for CEA detection to ensure the effectiveness of the CEA-detection process.

Detection and Analysis of CEA Tumor Marker. The existence of malignant tumors is one of the crucial factors that threaten human health.[51] CEA, which can be synthesized by tumor cells and early embryonic tissues, is a protein complex rich in polysaccharides that is closely related to tumors. Under normal circumstances, the content of CEA in adults is <5 ng mL^{-1}.[52] For the purpose of exploring the analysis performance of the OFET-based biosensor under illumination and darkness, different concentrations of CEA were analyzed by using the OFET-based biosensor. In this study, the OFET-based biosensor was developed to detect the changes of I_{DS} and V_{th} electrical signals induced by the immune reaction between antigen and antibody under illumination and darkness, respectively. Combined with the previous research,[29] due to the large size of the CEA antibody covering the surface of the organic semiconductor layer, the effective contact area of light was hindered to a certain extent, thereby reducing the photosensitivity of the OFET-based biosensor (Figure S7), but it did not affect the detection process of CEA (Figure S8).

The response signals under illumination of the OFET-based biosensor were obtained by the following formulas: $\Delta I_{DS} = (I_L - I_0)/I_0$ and $\Delta V_{th} = (V_L - V_0)/V_0$, and the response signals under darkness of the OFET-based biosensor were obtained by the following formulas: $\Delta I_{DS} = (I_D - I_0)/I_0$ and $\Delta V_{th} = (V_D - V_0)/V_0$, where I_0 and V_0 were the electrical signals measured under dark conditions before CEA incubation, I_D and V_D represented the electrical signals measured under dark conditions after CEA incubation, and I_L and V_L suggested the electrical signals measured under light conditions after CEA incubation. For the OFET-based biosensor under illumination, with the increment of the CEA concentration, the electrical-signal response triggered by CEA increased gradually for I_{DS} as the output signal (Figure 6a). In the range of 0.01−100 ng mL^{-1}, the linear regression equation for the I_{DS} signal and CEA solution was ΔI_{DS} = 51.44 log[C_{CEA} (ng mL^{-1})] + 168.2, accompanied by a linear correlation coefficient of 0.997. However, in the dark conditions of the OFET-based biosensor, the linear relationship for the I_{DS} signal and CEA solution was ΔI_{DS} = 4.24 log[C_{CEA} (ng mL^{-1})] + 5.35 in the range of 0.1−1000 ng mL^{-1}, accompanied by a linear correlation coefficient of 0.996 (Figure 6b). Compared with the I_{DS} response value in the dark conditions, the I_{DS} response value under illumination was significantly increased, which effectively improved the sensitivity to detect CEA. Also, the limits of detection for CEA were 13.5 fM and 0.5 pM under illumination and darkness conditions, respectively, using I_{DS} as the output signal.

Similarly, with V_{th} as the output signal, it also had good sensing performances for different concentrations of CEA. Under illumination, in the range of 0.01−100 ng mL^{-1}, the linear relationship for the V_{th} response and CEA solution was ΔV_{th} = 0.53 log[C_{CEA} (ng mL^{-1})] + 3.16, accompanied by a linear correlation coefficient of 0.996 (Figure 6c). Under darkness, the linear relationship for the V_{th} signal and CEA solution was ΔV_{th} = 0.18 log[C_{CEA} (ng mL^{-1})] + 0.35 in the range of 0.1−1000 ng mL^{-1}, accompanied by a linear correlation coefficient of 0.995 (Figure 6d). Under illumination and darkness conditions, the limits of detection for CEA

https://doi.org/10.1021/acs.analchem.1c03683
Anal. Chem. 2021, 93, 15167−15174

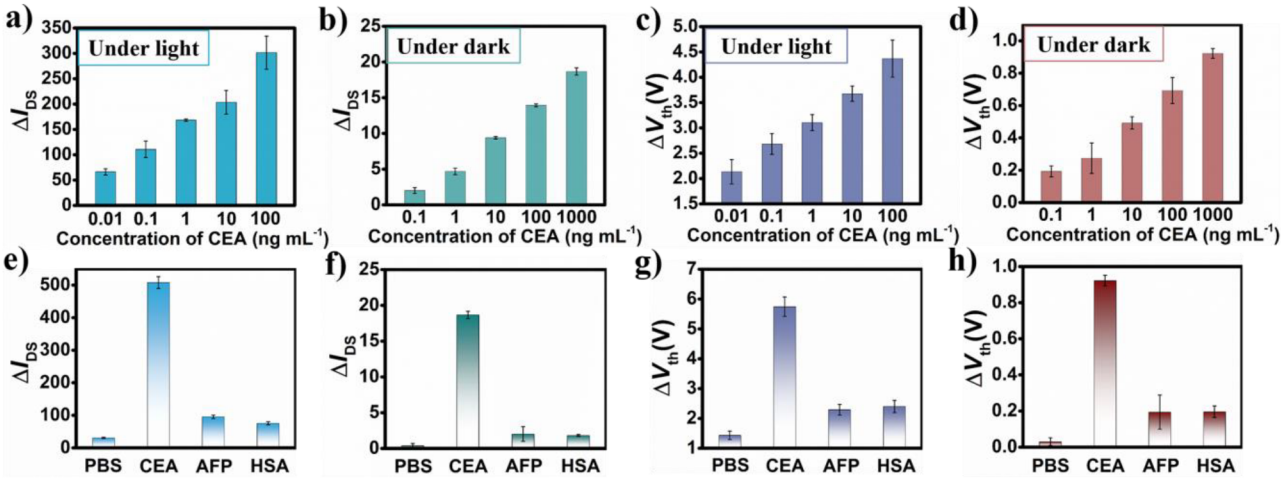

Figure 6. Bioassay of CEA with I_{DS} and V_{th} as the response signals. (a) Detection of the I_{DS} signal response caused by CEA solutions under illumination. (b) I_{DS} signal response induced by CEA solutions under darkness. (c) V_{th} signal response induced by CEA solutions detected under illumination. (d) V_{th} signal response induced by CEA solutions detected under darkness. (e) Selectivity of CEA detection under illumination for I_{DS} as response signal (1 × PBS; CEA, AFP, and HSA all in 1 μg mL^{-1}). (f) Selectivity of CEA detection under darkness for I_{DS} as response signal (1 × PBS; CEA, AFP, and HSA all in 1 μg mL^{-1}). (g) Selectivity of CEA detection under illumination for V_{th} as response signal (1 × PBS; CEA, AFP, and HSA all in 1 μg mL^{-1}). (h) Selectivity of CEA detection under darkness for V_{th} as the response signal (1 × PBS; CEA, AFP, and HSA all in 1 μg mL^{-1}). The error bar was the relative standard deviation obtained from 5 measurements (light source = 2.13 mW cm^{-2}, 808 nm).

were 16.9 fM and 0.2 pM, respectively, for V_{th} as the output signal. Compared with the results of CEA detection under darkness, the sensitivity of CEA detection under illumination was improved, which caused greater changes in the electrical signals of I_{DS} and V_{th} and was more conducive to the detection of CEA in low concentration. Moreover, this OFET-based biosensor endowed biological detection with a multisignal output function, so that different detection results can be mutually verified with higher reliability. In the future, sensors with multiple signal outputs are more conducive to the reliability of detection results, and it is also another strategy for researchers to construct innovative types of sensors.

It is worth noting that selectivity is also an important indicator for evaluating the sensor performance.[53] Under the same experimental conditions, the control experiments of α-fetoprotein (AFP), human serum albumin (HSA), and 1 × PBS further explored the specific recognition immune response of the OFET-based biosensor for CEA detection. AFP and HSA at a concentration of 1 μg mL^{-1} were detected under illumination (Figure 6e and g) and darkness (Figure 6f and h). The results showed that, when I_{DS} and V_{th} were selected as the response signals, the interference signal was almost negligible compared with CEA detection. Also, the 1 × PBS blank control experiment showed a weak response signal. It showed that the biosensor had acceptable selectivity for CEA detection. Therefore, the OFET-based biosensor reported in this Article has a good detection capability for CEA, and the multisignal output improves the reliability of the biosensor.

CONCLUSION

In summary, a new type of OFET-based biosensor was constructed in this study that used polymer PDQT with good photoelectric properties as both the photoelectric active layer and the biorecognition layer for high-sensitivity detection of CEA under illumination and darkness, respectively. Because light illumination promoted the transfer process of carriers and increased carrier concentration in the channel, making it easier to convert biological signals into higher electrical signals, the OFET-based biosensor exhibited higher sensitivity for CEA detection under illumination. The limits of detection were 13.5 and 16.9 fM with I_{DS} and V_{th} as the response signals, respectively, under illumination. At the same time, the limits of detection for CEA detection under darkness were 0.5 and 0.2 pM with I_{DS} and V_{th} as the response signals, respectively. In addition, multiple-signal output can be mutually verified, and it effectively improves the reliability of the biosensors. Therefore, on the basis of the advantages of small size, low cost, easy large-area fabrication, and easy integration, the biosensor is conducive to the high sensitivity and accuracy detection of some trace substances. This OFET-based biosensor has broad application prospects in the development of high-performance sensing platforms.

ASSOCIATED CONTENT

Supporting Information

The Supporting Information is available free of charge at https://pubs.acs.org/doi/10.1021/acs.analchem.1c03683.

Synthesis process of polymer PDQT, characterization of polymer PDQT, and related characterization of this OFET-based biosensor (PDF)

AUTHOR INFORMATION

Corresponding Author

Shanshan Cheng − *Tianjin Key Laboratory of Molecular Optoelectronic Sciences, Department of Chemistry, School of Science, Tianjin University, Tianjin 300072, P. R. China;* orcid.org/0000-0001-7282-2802; Email: chengss@tju.edu.cn

Authors

Xue Wang − *Tianjin Key Laboratory of Molecular Optoelectronic Sciences, Department of Chemistry, School of Science, Tianjin University, Tianjin 300072, P. R. China*

Chenfang Sun − *Tianjin Key Laboratory of Molecular Optoelectronic Sciences, Department of Chemistry, School of Science, Tianjin University, Tianjin 300072, P. R. China*

https://doi.org/10.1021/acs.analchem.1c03683
Anal. Chem. 2021, 93, 15167−15174

Congcong Zhang − *Institute for Advanced Interdisciplinary Research, University of Jinan, Jinan 250011, P. R. China*

Wenping Hu − *Tianjin Key Laboratory of Molecular Optoelectronic Sciences, Department of Chemistry, School of Science, Tianjin University, Tianjin 300072, P. R. China; Beijing National Laboratory for Molecular Science, Key Laboratory of Organic Solids, Institution of Chemistry, Chinese Academy of Sciences, Beijing 100190, P. R. China; Joint School of National University of Singapore and Tianjin University, Fuzhou International Campus, Tianjin University, Binhai New City, Fuzhou 350207, P. R. China;* orcid.org/0000-0001-5686-2740

Complete contact information is available at: https://pubs.acs.org/10.1021/acs.analchem.1c03683

Author Contributions

X.W.: Methodology, conceptualization, formal analysis, data curation, investigation, and writing of the original draft. C.S.: Methodology and review. C.Z.: Methodology. S.C.: Project administration, supervision, formal analysis, and writing review and editing. W.H.: Project administration and supervision. The manuscript was written through contributions of all authors, and all authors have given approval to the final version of the manuscript.

Notes

The authors declare no competing financial interest.

■ ACKNOWLEDGMENTS

The authors acknowledge financial support from the Ministry of Science and Technology of China (Grant nos. 2016YFB0401100, 2017YFA0204503, and 2015CB856502), and the National Natural Science Foundation of China (Grant nos. 21705116, 51733004, 91433115, 51633006, 51703160, 21661132006, and 21473222).

■ REFERENCES

(1) Villalonga, A.; Vegas, B.; Paniagua, G.; Eguilaz, M.; Mayol, B.; Parrado, C.; Rivas, G.; Diez, P.; Villalonga, R. *J. Electroanal. Chem.* **2020**, *877*, 114511.
(2) Wang, W.; Han, R.; Chen, M.; Luo, X. *Anal. Chem.* **2021**, *93*, 7355−7361.
(3) Cheng, S.; Hideshima, S.; Kuroiwa, S.; Nakanishi, T.; Osaka, T. *Sens. Actuators, B* **2015**, *212*, 329−334.
(4) Picca, R. A.; Manoli, K.; Luciano, A.; Sportelli, M. C.; Palazzo, G.; Torsi, L.; Cioffi, N. *Sens. Actuators, B* **2018**, *274*, 210−217.
(5) Magliulo, M.; Manoli, K.; Macchia, E.; Palazzo, G.; Torsi, L. *Adv. Mater.* **2015**, *27*, 7528−7551.
(6) Torsi, L.; Magliulo, M.; Manoli, K.; Palazzo, G. *Chem. Soc. Rev.* **2013**, *42*, 8612−8628.
(7) Sun, M.; Zhang, C.; Chen, D.; Wang, J.; Ji, Y.; Liang, N.; Gao, H.; Cheng, S.; Liu, H. *SmartMat* **2021**, *2*, 213−225.
(8) Shen, H.; Zou, Y.; Zang, Y.; Huang, D.; Jin, W.; Di, C.; Zhu, D. *Mater. Horiz.* **2018**, *5*, 240−247.
(9) Song, J.; Dailey, J.; Li, H.; Jang, H. J.; Zhang, P.; Wang, J. T. H.; Everett, A. D.; Katz, H. E. *Adv. Funct. Mater.* **2017**, *27*, 1606506.
(10) Mulla, M. Y.; Seshadri, P.; Torsi, L.; Manoli, K.; Mallardi, A.; Ditaranto, N.; Santacroce, M. V.; Di Franco, C.; Scamarcio, G.; Magliulo, M. *J. Mater. Chem. B* **2015**, *3*, 5049−5057.
(11) Lai, S.; Demelas, M.; Casula, G.; Cosseddu, P.; Barbaro, M.; Bonfiglio, A. *Adv. Mater.* **2013**, *25*, 103−107.
(12) Li, C.; Wu, H.; Zhang, T.; Liang, Y.; Zheng, B.; Xia, J.; Xu, J.; Miao, Q. *Chem.* **2018**, *4*, 1416−1426.
(13) Dai, H.; Gong, L.; Zhang, S.; Xu, G.; Li, Y.; Hong, Z.; Lin, Y. *Biosens. Bioelectron.* **2016**, *77*, 928−935.
(14) Xu, X.; Hou, R.; Gao, P.; Miao, M.; Lou, X.; Liu, B.; Xia, F. *Anal. Chem.* **2016**, *88*, 2386−2391.
(15) Lu, Y.; Zhao, H.; Fan, G.; Luo, X. *Biosens. Bioelectron.* **2019**, *142*, 111569.
(16) Liu, M.; Chen, G.; Qin, Y.; Li, J.; Hu, L.; Gu, W.; Zhu, C. *Anal. Chem.* **2021**, *93*, 9897−9903.
(17) Sun, C.; Li, R.; Song, Y.; Jiang, X.; Zhang, C.; Cheng, S.; Hu, W. *Anal. Chem.* **2021**, *93*, 6188−6194.
(18) Zhong, X.; Zhang, M.; Guo, L. a.; Xie, Y.; Luo, R.; Chen, W.; Cheng, F.; Wang, L. *Biosens. Bioelectron.* **2021**, *189*, 113389.
(19) Zhang, Q.; Fu, Y.; Xiao, K.; Du, C.; Zhang, X.; Chen, J. *Anal. Chem.* **2021**, *93*, 6801−6807.
(20) Sun, C.; Wang, X.; Auwalu, M. A.; Cheng, S.; Hu, W. *EcoMat* **2021**, *3*, No. e12094.
(21) Borges-Gonzalez, J.; Kousseff, C. J.; Nielsen, C. B. *J. Mater. Chem. C* **2019**, *7*, 1111−1130.
(22) Yang, F.; Sun, L.; Duan, Q.; Dong, H.; Jing, Z.; Yang, Y.; Li, R.; Zhang, X.; Hu, W.; Chua, L. *SmartMat* **2021**, *2*, 99−108.
(23) Zhou, K.; Dai, K.; Liu, C.; Shen, C. *SmartMat* **2020**, *1*, No. e1010.
(24) Sun, C.; Wang, Y.; Sun, M.; Zou, Y.; Zhang, C.; Cheng, S.; Hu, W. *Biosens. Bioelectron.* **2020**, *164*, 112251.
(25) Baeg, K.; Binda, M.; Natali, D.; Caironi, M.; Noh, Y. *Adv. Mater.* **2013**, *25*, 4267−4295.
(26) Xie, C.; Mak, C.; Tao, X.; Yan, F. *Adv. Funct. Mater.* **2017**, *27*, 1603886.
(27) Xie, C.; Yan, F. *Small* **2017**, *13*, 1701822.
(28) Lei, Y.; Li, N.; Chan, W. K. E.; Ong, B. S.; Zhu, F. *Org. Electron.* **2017**, *48*, 12−18.
(29) Jiang, X.; Sun, C.; Zhang, C.; Cheng, S. Highly responsive biosensors based on organic field-effect transistors under light irradiation. *Chin. Chem. Lett.* 2021, DOI: 10.1016/j.cclet.2021.04.005 (accessed Apr 3, 2021).
(30) Woo, K.; Kang, W.; Lee, K.; Lee, P.; Kim, Y.; Yoon, T. S.; Cho, C. Y.; Park, K. H.; Ha, M. W.; Lee, H. H. *Biosens. Bioelectron.* **2020**, *159*, 112186.
(31) Gu, P.; Hu, M.; Ding, S.; Zhao, G.; Yao, Y.; Liu, F.; Zhang, X.; Dong, H.; Wang, X.; Hu, W. *Chin. Chem. Lett.* **2018**, *29*, 1675−1680.
(32) Li, Y.; Sonar, P.; Singh, S. P.; Soh, M. S.; van Meurs, M.; Tan, J. *J. Am. Chem. Soc.* **2011**, *133*, 2198−2204.
(33) Ha, J. S.; Kim, K. H.; Choi, D. H. *J. Am. Chem. Soc.* **2011**, *133*, 10364−10367.
(34) Seshadri, P.; Manoli, K.; Schneiderhan-Marra, N.; Anthes, U.; Wierzchowiec, P.; Bonrad, K.; Di-Franco, C.; Torsi, L. *Biosens. Bioelectron.* **2018**, *104*, 113−119.
(35) Yang, N. J.; Liao, C. S.; Chen, S. A. *Adv. Funct. Mater.* **2010**, *20*, 1000−1004.
(36) Chen, H.; Guo, Y.; Yu, G.; Zhao, Y.; Zhang, J.; Gao, D.; Liu, H.; Liu, Y. *Adv. Mater.* **2012**, *24*, 4618−4622.
(37) Sun, C.; Vinayak, M. V.; Cheng, S.; Hu, W. *Anal. Chem.* **2021**, *93*, 11305−11311.
(38) Yao, Y.; Chen, Y.; Wang, H.; Samorì, P. *SmartMat* **2020**, *1*, No. e1009.
(39) Angione, M. D.; Cotrone, S.; Magliulo, M.; Mallardi, A.; Altamura, D.; Giannini, C.; Cioffi, N.; Sabbatini, L.; Fratini, E.; Baglioni, P.; Scamarcio, G.; Palazzo, G.; Torsi, L. *Proc. Natl. Acad. Sci. U. S. A.* **2012**, *109*, 6429−6434.
(40) Li, H.; Shi, Y.; Han, G.; Liu, J.; Zhang, J.; Li, C.; Liu, J.; Yi, Y.; Li, T.; Gao, X.; Di, C.; Huang, J.; Che, Y.; Wang, D.; Hu, W.; Liu, Y.; Jiang, L. *Angew. Chem., Int. Ed.* **2020**, *59*, 4380−4384.
(41) Huang, Y.; Wu, C.; Chuang, C.; Pang, S.; Pan, T.; Yang, Y.; Ko, F. *Anal. Chem.* **2013**, *85*, 7912−7918.
(42) Ji, D.; Li, T.; Liu, J.; Amirjalayer, S.; Zhong, M.; Zhang, Z.; Huang, X.; Wei, Z.; Dong, H.; Hu, W.; Fuchs, H. *Nat. Commun.* **2019**, *10*, 12.
(43) Wasapinyokul, K.; Milne, W. I.; Chu, D. P. *J. Appl. Phys.* **2011**, *109*, 084510.
(44) Abraham, G. K.; Pal, B. B.; Khan, R. U. *IEEE Trans. Electron Devices* **2000**, *47*, 1469−1471.

(45) Tao, J.; Liu, D.; Qin, Z.; Shao, B.; Jing, J.; Li, H.; Dong, H.; Xu, B.; Tian, W. *Adv. Mater.* **2020**, *32*, 1907791.
(46) Liu, X.; Guo, Y.; Ma, Y.; Chen, H.; Mao, Z.; Wang, H.; Yu, G.; Liu, Y. *Adv. Mater.* **2014**, *26*, 3631−3636.
(47) Luo, X.; Du, L.; Liang, Y.; Zhao, F.; Lv, W.; Xu, K.; Wang, Y.; Peng, Y. *ACS Appl. Mater. Interfaces* **2018**, *10*, 15352−15356.
(48) Hideshima, S.; Sato, R.; Inoue, S.; Kuroiwa, S.; Osaka, T. *Sens. Actuators, B* **2012**, *161*, 146−150.
(49) Cheng, S.; Hotani, K.; Hideshima, S.; Kuroiwa, S.; Nakanishi, T.; Hashimoto, M.; Mori, Y.; Osaka, T. *Materials* **2014**, *7*, 2490−2500.
(50) Chu, C.; Sarangadharan, I.; Regmi, A.; Chen, Y.; Hsu, C.; Chang, W. H.; Lee, G. Y.; Chyi, J. I.; Chen, C. C.; Shiesh, S.; Lee, G. B.; Wang, Y. *Sci. Rep.* **2017**, *7*, 5256.
(51) Wang, W.; Wang, Q.; Xie, H.; Wu, D.; Gan, N. *Talanta* **2021**, *222*, 121456.
(52) Iwanaga, M. *ACS Nano* **2020**, *14*, 17458−17467.
(53) Han, Q.; Wang, R.; Xing, B.; Zhang, T.; Khan, M. S.; Wu, D.; Wei, Q. *Biosens. Bioelectron.* **2018**, *99*, 493−499.

https://doi.org/10.1021/acs.analchem.1c03683
Anal. Chem. 2021, 93, 15167−15174